A PEG-PLGA-based polymeric capsule as theranostic nanoplatform for active targeting atherosclerosis

Chen Jiandong (chenjdcardiologist@njucm.edu.cn)
Jiangsu province hospital of china medicin

Weixin Sun
Jiangsu Province Hospital of Chinese Medicine

Xinzhu Li
Jiangsu Province Hospital of Chinese Medicine

Xin Lu
Jiangsu Province Hospital of Chinese Medicine

Peng Yu
Jiangsu Province Hospital of Chinese Medicine

Le Shen
Jiangsu Province Hospital of Chinese Medicine

Xiaohu Chen
Jiangsu Province Hospital of Chinese Medicine

Research

Keywords: atherosclerosis, active targeting, molecular imaging, nano-carrier

Posted Date: July 24th, 2020

DOI: https://doi.org/10.21203/rs.3.rs-44350/v1

Abstract

Background Atherosclerosis plaque is a major cause of cardiovascular diseases across the globe, which is characterized by a gradual formation of atherosclerotic plaque, hardening, and narrowing of the arteries. Nano-materials can serve as powerful delivery platforms for atherosclerosis treatment. Herein we systematically developed polymeric capsule with active targeting property encapsulating curcumin (Cur) and C-C chemokine receptor type 2 with short-interfering RNA (CCR2-siRNA) for combined treatment, which was also loaded with Gd^{3+} for magnatic resonance imaging (MRI) and a near-infrared fluorochrome (IR780) for fluorescence imaging (FI).

Results The resulting nano-capsule exhibited a favorable hydrodynamic size and negative surface charge. More importantly, the negative charge and active-targeting peptide resulted in enhanced accumulation of nano-capsule in the established atherosclerotic plaques, thereby achieving targeted drug release. The *in vitro* and *in vivo* results indicated the effective diagnostic and therapeutic sensitivity, which could promote the development of theranostics for clinical implementation.

Conclusions This study demonstrated that chemotherapy combined with gene therapy can displayed synergistic effect in atherosclerosis treatment, which possessed efficient management of atherosclerosis.

Introduction

Atherosclerosis is a progressive inflammatory disease which leads to the hardening and thickening of the arterial walls [1–4]. It is initiated by the dysfunction of endothelial cells, which subsequently promotes the proliferation of vascular smooth muscle cells and reconstruction of extracellular matrix, ultimately leading to the formation of plaques, which are comprised of lipids, immune cells, and fibrous elements [5]. It is a predominant cause of a variety of cardiovascular disorders including myocardial infarction, ischemic stroke, and peripheral vascular disease and accounts for significant morbidity and mortality rates in the aged population, especially in industrialized countries [6, 7].

There are generally no symptoms in the early stages of atherosclerosis and traditional detection techniques cannot easily, safely, and effectively detect the lesions in the early stages [8, 9]. In recent years, there has been a rapid development in using nano-carrier technique as a tool for molecular imaging of atherosclerotic lesion [10–12]. By incorporating peptides, antibodies, or other ligands on its surface, a nano-carrier can target adhesion molecules in lesion components. Engineering supramolecular micelles exhibit promising characteristics for the diagnosis of the disease by targeting cellular components in atherosclerotic plaques, such as endotheliocyte [13]. In our research, we developed peptide-conjugated PEG-PLGA nano-capsule to target vascular cell adhesion molecule-1 (VCAM-1) expressed by endothelial cells, which incorporated anti-inflammatory Cur and CCR2-siRNA for combined therapy. CCR2-siRNA enabled silencing of C-C chemokine receptor type 2 (CCR2), which was the chemokine receptor that dominated recruitment of inflammatory monocytes [14]. Moreover, encapsulated resonance contrast agent Gd^{3+} and near-infrared light dye IR780 can be also delivered to atherosclerotic plaques by virtue of its

specific binding ability to endothelial cells, and thus could be utilized as a tool for imaging observation and diagnosis of the disease. The purpose of this study was to evaluate the distribution of nano-drug in a mouse atherosclerosis model *in vivo*. The nanoparticles could specifically bind to the atherosclerosis plaque, due to the specific interaction of VCAM-1 and endothelial cells in the plaque. After binding, Cur and siRNA were successively released to treat the atherosclerosis plaque.

Materials And Methods

Materials

Poly (lactic-co-glycolic acid) - carboxyl poly (ethylene glycol) ($PLGA_{10k}$ - PEG_{5k} - COOH) was obtained from Shandong institute of medical devices, China. Poly (vinyl alcohol) (PVA, 88%, M_w=31000) was purchased from Acros Organics. IR780 iodide and alpha-tocopheryl poly (ethylene glycol) 1000 Succinate (TPGS) were purchased from Sigma Company. Curcumin was purchased from Aladin Company. VCAM-1 polypeptide was supported by ChinaPeptides Co., Ltd, China. All other reagents and solvents were purchased from Sinopharm Chemical Reagent Co., Ltd., China.

Preparation Of Blank Plga-peg-cooh Capsule (bpc)

PLGA-PEG-COOH capsule were prepared by the double emulsion (W/O/W) method with a little modification. Briefly, 50 mg of $PLGA_{10K}$-PEG_{5K}-COOH dissolved in 1 mL of chloroform and 6 mL of aqueous solution containing 1% mixture of PVA and TPGS (outer aqueous phase, PVA : TPGS = 1:5) were transferred to a centrifuge tube, and the mixture was emulsified by sonication for 2 min (80W) in an ice bath. Then the emulsion was then slowly dropped into 30 mL of 0.3% PVA and stirred overnight to volatilize chloroform and solidify the surface of the PLGA ball. After evaporation of the solvent, the samples were transferred to microsep (cut off: 100 KD) for ultrafiltration cleaning and diluted into 5 mL of deionized water kept in 4 °C. The sample was died and weighed to calculate the concentration and solid content.

Preparation of PLGA-PEG-COOH capsule containing IR780, Cur, CCR2-siRNA and Gd^{3+} (PC_S)

Cur, IR780 and $PLGA_{10K}$-$mPEG_{5K}$ were dissolved respectively in chloroform and prepared into 20, 10, and 100 mg/mL solution. 50 μL of curcumin solution, 50 μL of IR780 solution, and 500 μL of $PLGA_{10K}$-$mPEG_{5K}$ solution were transferred to a centrifuge tube, and the mixture was emulsified by sonication for 2 min (80W) in an ice bath prepared for use. 5 nmol of CCR2-siRNA was dissolved in 50 uL of diethy pyrocarbonate (DEPC) aqueous solution (2% Gd^{3+}) as the internal water phase, and colostrum was formed by ultrasonication with a probe in an ice bath for 2 min. The formed colostrum was added to

6 mL of aqueous solution containing 1% mixture of PVA and TPGS (outer aqueous phase, PVA: TPGS = 1:5), and ultrasonicated for 2 minutes (80 W) in an ice bath to form double emulsion (W/O/W). Then the emulsion was dispersed into 30 mL of 0.3% PVA solution and stirred overnight to volatilize chloroform and solidify the surface of the PLGA ball. After evaporation of the solvent, the samples were transferred to microsep (cut off: 100 KD) for ultrafiltration cleaning and diluted into 5 mL of deionized water kept in 4 °C. The sample was died and weighed to calculate the concentration and solid content. PLGA-PEG-COOH capsule containing IR780, Cur, and Gd^{3+} was also constructed in the similar method and denoted as PC.

Preparation of PLGA-PEG-COOH capsule modified with VCAM-1 polypeptide containing IR780, Cur, CCR2-siRNA and Gd $^{3+}$ (PC_{SV})

1 mL of PLGA-PEG-COOH capsule (PC or PC_S, 10 mg/mL) was centrifuged and dispersed into 0.5 mL of 2-morpholinoethanesulfonic acid (MES) (100 mM, pH 4.8), following adding VCAM-1 peptide (300 μg) at 37 °C. After adsorption for 1 h. 80 μL of 1-(3-Dimethylaminopropyl)-3-ethylcarbodiimide hydrochloride (EDC) solution was added for coupling at 37 °C overnight, which was prepared in MES solution (100 mM) and adjusted into the concentration of 240 mg/mL. The treated sample was purified by centrifugation with deionized water, and stored in 4 °C before use. PC and PC_S conjugated with VCAM-1 peptide were denoted as PC_V and PC_{SV}, respectively.

Characterization Of Nano-capsule

The size and zeta potential of BPC, PC_S and PC_{SV} vesicles were determined using a Malvern Zetasizer Nano ZS unit (Nano ZS 90, Malvern, UK) with a He-Ne laser (λ = 633 nm) at a scattering angle of 90° at 25 °C. A drop of BPC, PC_S or PC_{SV} solution was dropped onto a copper mesh, and stained by 1% phosphotungstic acid. Subsequently, the morphology of BPC, PC_S and PC_{SV} solution were visually observed using a transmission electron microscope at 200 kV (TEM, JEM-2100F, JEOL, Japan).

Drug loading and in vitro drug release study

To calculate the loading efficiency of PC_{SV}, lyophilized powder was dissolved and measured by UV-vis spectrophotometer (DU730, Beckman Coulter). Briefly, lyophilized powder was dissolved in DMSO, and the absorbance measured at 440 nm to obtain Cur loading efficiency. Likewise, lyophilized powder was dissolved in DEPC aqueous solution, and the absorbance measured at 260 nm and 280 nm to obtain CCR2-siRNA loading efficiency. According to the pre-established standard curve of Cur and CCR2-siRNA

(Figure S1, S2), the drug-loading content (DLC) and drug-loading efficiency (DLE) of nanoparticles were calculated by the following equations.

$$DLC\% = \frac{\text{weight of drug in nanopartic les}}{\text{weight of drug loaded nanoparicl es}} \times 100\% \quad (1)$$

$$DLE\% = \frac{\text{experiment al drug loading}}{\text{theoretica l drug loading}} \times 100\% \quad (2)$$

To study the drug release profile *in vitro*, PC_S and PC_{SV} nanoparticle solutions (1 mL) were added to disposable dialysis cups (Slide-A-Lyzer MINI Dialysis Units, MWCO:3500 Da, Thermo Scientifc) in PBS (10 mL). At different time points, the external drug and gene release buffers were collected and an equivalent amount of PBS was added. The cumulative amount of Cur and siRNA released was quantified by UV-vis spectrophotometer.

Cellular Binding And Uptake Tests

The murine bEnd.3 cells were seeded in 12-well plates at a density of 1×10^5 cells per well in 1 mL of DMEM medium containing 10% FBS, and cultured at 37 °C with 5% CO_2 for 24 h. When the cells reached 60–70% confluence, 3 ng/mL tumor necrosis factor-α (TNF-α) was added and further incubated for 12 h. PC_{SV} were added to the TNF-α-stimulated cell monolayer. After incubation for 1 h, the cells were washed with PBS, and fixed with paraformaldehyde (4% in PBS). The nuclei of the cells were stained with DAPI. The cells were observed using fluorescence microscope.

Inhibition of proliferation of macrophages

in vitro

RAW264.7 cells were seeded in a 96-well plate (5000 cells per well), and cultured in DMEM medium containing 0.5% FBS for 12 h. Then, the cells were incubated with various doses of free Cur, PC_S, and PC_{SV} for 24 h, respectively. The cell viability was quantified by CCK-8 assay.

Establishment of atherosclerosis model

in vivo

Male apolipoprotein E-deficient (ApoE-/-) mice (25–30 g, eight-week old) were obtained from the Third Military Medical University in Chongqing, China. The mice were fed with high-fat (0.2% cholesterol, 21% fat) diet (HFD) for 14 weeks to establish the classical atherosclerosis model.

Distribution of nanoparticles

in vivo

ApoE-/- mice were fed with a high fat diet (HFD) for 14 weeks, mice in the HFD group were randomly divided into three groups with four mice in each group. They were separately injected with PBS (0.01 M, pH = 7.4), PC_V (0.6 mg Cur/kg, 5 mg Gd^{3+}/kg) and PC_{SV} (0.6 mg Cur/kg, 5 mg Gd^{3+}/kg) via tail vein injections on days 1, 3, and 5. On day 4, the atherosclerosis in the thoracoabdominal aorta of the mice was examined by MRI coronal reformatted imaging using the 3.0 T GE MRI system using a fast spin echo sequence. For quantitative analysis, we calculated the signal-to-noise ratio (SNR) in the same 3 regions of interest placed in the aortic wall of the lower intrathoracic aorta on 3 different coronal reformatted images. For *in vivo* whole-body NIRF imaging, the IR780 fluorescence from the anesthetized mice were collected by using a Bruker *In Vivo* Xtreme imaging system with 704 nm excitation and 740 nm emission filters. After *in vivo* imaging, the mice were sacrificed and perfused with 10 mL of PBS by injection through the left ventricle. The aorta, heart, liver, spleen, pancreas, and kidney were imaged *ex vivo* to obtain quantitative photon counts of their NIRF intensities.

Histology And Immunohistochemistry

ApoE-/- mice were randomized into 4 groups (four mice per group), and given the HFD for 14 weeks. Then, the mice were subjected to the different treatments for one month. The mice injected with 5% sucrose served as the control group, while the other three groups were treated with either free drug, PC_V or PC_{SV} at a dose of 0.7 mg/kg of Cur every two days via tail vein injection. The body weight of mice was monitored every two days during the treatment to evaluate the systemic toxicity. After treatment for 30 day, the aortas, from the heart to the iliac bifurcation, were harvested. The aortic roots were fixed with paraformaldehyde (4% in PBS) for 1 h, and then prepared to paraffin sections. After deparaffinizing, Masson's trichrome and Toluidine blue staining were used to quantify the content of collagen and the necrotic core, respectively. For immunohistochemistry analysis, Sections of the main organs including aortas, heart, liver, spleen, lung, and kidney were also analyzed by hematoxylin-eosin (HE) staining.

Complete Blood Biochemistry And Routine Analysis

Blood was collected in EDTA2K spray-coated tubes after treatment for one month, and immediately analyzed using an automated hematology analyzer (Sysmex KX-21, Sysmex Co., Japan). The concentrations of alanine aminotransferase and aspartate aminotransferase in plasma from different treatments were quantified by an automated analyzer platform (Roche Cobas C501, Roche Co., Switzerland).

Statistical analysis

The results were presented as mean ± standard deviation (SD). Statistical significance was analyzed using Student's t-test.

Results And Discussion

Fabrication and characterization of vesicles

Efficient solubilization is critical for hydrophobic Cur to reach a sufficient dose in the atherosclerotic lesion [15, 16]. We, therefore, generated PC_{SV} by encapsulating the hydrophobic Cur into the hydrophobic capsule of PLGA using a micro-emulsion method. In contrast to the saturation solubility of Cur in water (only ≈ 6 μg / mL), we were able to load 117 μg of Cur into 1 mL of PLGA aqueous solution (117 μg / mL), thereby dramatically increasing its solubilization (more than 15 times greater than in water). As shown in Table S2, DLE and DLC of PC_{SV} were 0.9% and 58.5%, respectively. For CCR2-siRNAs, DLE and DLC of PC_{SV} were 0.228% and 100%, respectively.

Next, we first examined the hydrodynamic diameters (D_h) of BPC, PC_S and PC_{SV} by DLS. As shown in Fig. 1, encapsulating IR780, CCR2-siRNA, Cur, and Cd^{3+} increased the mean D_h from 172.5 ± 8.6 nm (BPC, Polydispersity index (PDI): 0.208) to 191.4 ± 11.3 nm (PC_S, PDI: 0.125). This increase in D_h was consistent with the embedding of the particles with inner water phase. The D_h of PC_{SV} was close to that of PC_S, suggesting that the peptide coupling the surface of particles had little effect on particle size. Moreover, PC_{SV} showed a relatively constant hydrodynamic diameter after long-term storage at room temperature, indicating its favorable stability properties (Fig.S3). This good stability of nano-carrier in physiological condition was important and beneficial for their *in vivo* application and intravenous injection [17–19]. In addition, surface zeta potential analysis showed that BPC had a zeta potential of − 20.8 ± 0.8 mV, whereas PC_S (− 25.4 ± 1.5 mV) and PC_{SV} (− 38.8 ± 1.7 mV) have lower values (Fig. 1d, e, f). The targeting polypeptide conjugated nano-carriers further decreased the zeta potential, enabling long circulation to the plaque sessions. Since the physiochemical properties of all the nano-carriers in this study were similar, it was reasonable to presume that their ability to target atherosclerotic plaque would be dominated by the targeting ligand.

We further analyzed the morphologies of BPC, PC_S and PC_{SV} using TEM. Both nanoparticles showed a uniform sphere morphology. Moreover, they displayed a clear capsule nanostructure without conspicuous interconnection (Fig. 1g, h, i), which confirmed that the W/O/W emulsion nanostructure was successfully prepared. To verify the IR780 encapsulated in the nano-carrier, fluorescent images of BPC, PC_S and PC_{SV} was displayed as Fig. 2a. This fluorescent intensity suggested that IR780 were strongly retained on the inside of PC_S and PC_{SV}.

We designed drug and siRNA codelivery system, loading drug and siRNA by emulsion methods, which was a classic method for the preparation of nanoparticles [20, 21]. The *in vitro* release of Cur from the nanoparticles was investigated in PBS (pH 7.4) solution to simulate the physiological environment

(Fig. 2b). A fast release of Cur from both nanoparticles was observed in the initial 24 h (> 20%). After 60 h incubation in PBS, 44.2% of Cur was released from PC_S nanoparticle, while 39.8% of Cur was released from the PC_{SV} nanoparticle. When compared with the PC_S nanoparticles, PC_{SV} nanoparticles showed a slightly slower Cur release profile, which may be ascribed to the additional polypeptide in the outer sphere acting as a diffusion barrier [21].

The release curves of siRNA from PC_S and PC_{SV} nanoparticles were similar, and these were because the siRNA were encapsulated in the inner layer of the capsules, which could be extended released readily [22]. In contrast to Cur release profiles, there was a considerable delay in the release of siRNA from the PC_S and PC_{SV}, especially during the first 4 h, during which almost none of the loaded siRNA was released (Fig. 2c). After 60 h, only 18.9% and 17.8% of siRNA loaded in the PC_S and PC_{SV} had been released, respectively. This delayed release of siRNA was likely due to the fact that siRNA was loaded only in inner aqueous phase. These results demonstrated that the design of nanoparticles with spatially segregated Cur in the outer oil layer and siRNA in the aqueous core was verified for successfully prepared.

In vitro macrophage inhibition and endothelial cell adhesion of nanoparticles

The cytotoxicity of the nanoparticles was evaluated in the macrophages. As shown in Figure 2d, all nanoparticles showed a dose-dependent cytotoxicity in RAW264.7 cells. To evaluate the *in vitro* cytotoxicity quantitatively, we calculated the IC_{50} of the nanoparticles, defined as the drug concentration required to kill 50% of the incubated cells. BPC, which was not loaded with Cur, did not show any cytotoxic effect (with an IC_{50} of >100 μg/mL) (Fig.S4). As expected, the cytotoxic effect of PC_V (IC_{50}: 6.35 μg/mL) did not differ from that of PC_{SV} (6.87 μg/mL). These results suggested that PC_V and PC_{SV} were comparable in inhibition of macrophage proliferation. In contrast, at the same dose, the slightly more potent antiproliferative activity of free Cur (IC_{50}: 4.60 μg/mL) might be ascribed to the slower Cur release from PLGA of PC_V or PC_{SV} [23].

Moreover, bEnd.3 cells were used to develop the *in vitro* inflammatory cell model by stimulating with appropriate concentration of TNF-α. The expression level of VCAM-1 was gradually increased with the increase in TNF-α concentration [13, 24]. In order to examine the targeting adhesion of these nanoparticles to the inflammatory cells, bEnd.3 cells were pre-incubated with TNF-a at a concentration of 3 ng / mL for 12 h then further incubated with PC_{SV} for an additional 1 h. Fig.3 showed representative bright-field micrographs of these nanoparticles bound to cells, revealing that these targeted nanoparticles can bind the TNF-α-stimulated cells. Importantly, the number of nanoparticles bound to the stimulated cells increased with the addition of TNF-α, which indicated that the cell affinity of nanoparticles to the stimulated cells can infer the cell inflammation degree.

Organ-level distribution of PC_V and PC_{SV}

As silencing of CCR2, the monocytic chemokine receptor responsible for migration of the inflammatory monocyte subset to sites of inflammation can be realized by using siRNA technology, siRNA silencing of CCR2 (siCCR2) significantly can attenuate receptor protein expression in circulating and splenic monocytes [14]. We investigated the *in vivo* MRI efficacy of PC_V and PC_{SV} via comparison of scans obtained pre-injection and at treatment with agent injected into the tail vein of atherosclerotic mice on day 4. MRI revealed pronounced and heterogeneously distributed hyper-intense areas throughout plaque-rich regions in the abdominal aorta after administration of nanoparticles. A representative example of the results of imaging ApoE-/- mice with PC_V and PC_{SV} were shown in Fig.4a. A clear and significant enhancement of image density was observed in the aorta wall post-injection in PC_V and PC_{SV}, indicating that nanoparticles attached with VCAM1 binding peptide was successful in targeting the plaques and enhancing them in MR images [25-27]. By comparison, the MR signal of PC_{SV} was lowered than that of PC_V after administration of nanoparticles. It indicated that intervention of siRNA lowered the MRI signal in association with attenuated monocyte recruitment. Therefore, the aortic section of siCCR2 treated ApoE-/- mice had decreased MR signal. Adoption of the medical image-analysis software package eFilm allowed the signal intensity to be ascertained and the percent change in normalized enhancement ratio post-injection to be calculated. The results of this analysis were displayed in Fig.4b. The data confirmed the visual impression that PC_V was an effective agent for the enhancement of images of the wall of the aorta of ApoE-/- mice, giving an enhancement of 11%, while that of PC_{SV} was only 6%, which showed that the PC_V was targeted more effectively to atherosclerotic lesions [28].

We also monitored the organ-level distribution of PC_V and PC_{SV} by utilizing IR780-labeled capsules. ApoE-/- mice received treatment of PC and PC_V on day 4, followed by the performance of *in vivo* NIRF imaging of the animals (Fig.4c) and *ex vivo* NIRF imaging of the excised organs (Fig.4d). For PC_{SV} group, we observed stronger signals in the liver and lung and *ex vivo* imaging analysis revealed the most-intense IR780 fluorescence in the liver among all of the organs. Other organs with a noticeable accumulation of PC were the lung, kidney, spleen. For the PC_V group, *in vivo* and *ex vivo* NIRF imaging data also showed strong fluorescence in the liver, lung, and spleen. Our NIRF imaging data suggested the more accumulation of PC_V in heart and aorta than that of PC_{SV} (Fig.4e), which reconfirmed decrease of VCAM1 in the PC_{SV} group. As VCAM1-binding peptide conjugation enabled high targeting capability of the nanoprobe to the inflamed endothelium expressing VCAM1 in a high plaque regions [29], the decreased endothelium expressing VCAM1 attenuated targeting of peptide, thus lowered the intensity of NIRF imaging. The results of MR and FI all implied that there was a more favorable therapeutic effect in PC_{SV} compared with PC_V group in the process of treatment.

In Vivo target atheroprotective effect

We detected the composition of atherosclerotic plaque in aortic root sections by immunohistochemistry staining. The results showed that the atherosclerosis plaque in the PC_V and PC_{SV} group disappeared on the whole, and no plaque rupture was observed. In contrast, other groups (control and Cur) displayed obvious atherosclerosis plaque and plaque rupture was observed in saline-treated groups (Fig.5a).

The necrotic areas in the aortic roots were detected by toluidine blue staining. As shown in Fig.5b, the control group exhibited large necrotic areas with substantial cholesterol crystals, indicating advanced lesions. After treatment with Cur, PC_V and PC_{SV}, the necrotic area was significantly decreased. Quantitative analysis revealed that, compared to the control group, the average necrotic area was decreased to 14.5%, 7.3%, and 5.2% in response to free Cur, PC_V, and PC_{SV} treatment, respectively (Fig.5c). The increased collagen produced by hyperplasia smooth muscle cells leads to the enlargement of the plaque areas, which could further narrow the vascular lumen [30, 31]. We tested the content of collagen in plaque areas using Masson's trichrome staining (Fig.5d). Compared to the control, free Cur, PC_V, and PC_{SV} effectively decreased the content of collagen. Quantitative analysis revealed that, compared to the control group, the average content of collagen was decreased to 20.5%, 14.3%, and 11.2% in response to free Cur, PC_V, and PC_{SV} treatment, respectively (Fig.5e). Therefore, PC_V and PC_{SV} all exhibited preferable therapy on the plaque in ApoE-/-mice by reducing necrotic area and collagen deposition. Due to intervention of siRNA, PC_{SV} can achieve more favorable therapeutic effect, leading to a more decreased plaque index [32].

Biosafety Assessment

To assess biosafety, adverse effects were studied after treatment for one month. There was less 10% body weight loss in free Cur, while no significant difference in body weight of mice was observed in PC_V and PC_{SV} groups (Fig.6a). The mice receiving various treatments showed no significant change in the weight compared to that of untreated control, which showed that mice exhibited tolerance to all the treatments. Moreover, as the nano-capsules accumulated in the liver, the effect of liver was needed to be verified. No obvious difference in the liver index of suggested no significant toxicity, and the liver index of the group treated with PC_V gradually returned, which was closed to normal level. The blood biochemical assays of alanine aminotransferase (ALT) and aspartate aminotransferase (AST), were at normal levels, which indicated that the functions of the liver were not impaired by the treatment (Fig.6b,c) [24, 31]. Therefore, PC_{SV} did not induce significant adverse effects in long-term treatment, indicating its potential as a safe candidate for chronic vascular disease therapy. The results of hematoxylin-eosin (H&E) staining showed that no noticeable pathological changes could be found in the main organs, which further confirmed their biocompatibility (Fig.6d).

Conclusions

In summary, we developed polymeric capsule with active targeting encapsulating Cur and CCR2-siRNA for combined treatment, which was loaded with Gd^{3+} for MRI and a near-infrared fluorochrome (IR780) for FI.

The resulting nanoparticle (PC_{SV}) showed favorable properties including controllable size, negative charge, and effective inhibition of macrophage proliferation and active target of endothelial cells *in vitro*. In ApoE-/- mice model which induced atherosclerosis by a high-fat diet, PC_{SV} nanoparticles accumulated in established atherosclerotic plaques. Compared with PC_V, PC_{SV} significantly delayed the progression of atherosclerosis after treatment for one month. Furthermore, the nanoparticles displayed a desirable safety profile without significant side effects, even after long-term administration in mice. Overall, the nanoparticles may be considered as a feasible candidate for a new class of safe and effective targeted drug delivery system for chronic inflammatory disease management.

Abbreviations

CCR2: C-C chemokine receptor type 2; VCAM-1:vascular cell adhesion molecular-1; DLC:drug-loading content; DLE:drug-loading efficiency; TEM:Transmission electron microscopy; DLS:dynamic light scattering; NIRF:near-infrared fluorescence.

Declarations

Authors' contributions

Jiandong Chen drafted the manuscript, performed the experiment and analyzed the data. Weixin Sun performed the chemical experiment, analyzed the data and modified the manuscript. Xinzhu Li and Xin Lu performed the cellular experiment, analyzed the data. Peng Yu and Le Shen performed animal model and analyzed the data. Jiandong Chen and Xiaohu Chen conceived, designed the study and thereafter supported experimental guidance and modification of manuscript.

Author details

Jiangsu province Hospital of Chinese Medicine, Affiliated to Nanjing University of Chinese Medicine, Nanjing, 210029, China.

Acknowledgements

Not applicable.

Competing interests

The authors declare no competing financial interest.

Availability of data and materials

All data generated or analyzed during this study are included in the article and additional file. The additional file is available.

Consent for publication

All authors have provided consent for the manuscript to be published.

Ethical approval

All experiments in the research were conducted under a protocol approved by the Institutional Animal Care and Use Committee at Southeast University, China.

Funding

The authors are grateful for the financial support provided by the National Natural Science Foundation of China (No. 81973763) and Six Talent Peaks Project in Jiangsu

Province (No.WSN018).

References

1. Weber C, Noels H. Atherosclerosis. Current pathogenesis and therapeutic options. Nat Med. 2011;17:1410–22.
2. Feig JE, Parathath S, Rong JX, Mick SL, Vengrenyuk Y, Grauer L, et al. Reversal of hyperlipidemia with a genetic switch favorably affects the content and inflammatory state of macrophages in atherosclerotic plaques. Circulation. 2011;123:989–98.
3. Williams KJ, Feig JE, Fisher EA. Rapid regression of atherosclerosis: Insights from the clinical and experimental literature. Nat Clin Pract Cardiovasc Med. 2008;5:91–102.
4. Sanchez-Gaytan BL, Fay F, Lobatto ME, Tang J, Ouimet M, Kim Y, et al. HDL-Mimetic PLGA Nanoparticle To Target Atherosclerosis Plaque Macrophages. Bioconjug Chem. 2015;26:443–51.
5. Tabas I. Macrophage death and defective inflammation resolution in atherosclerosis. Nat Rev Immunol. 2010;10:36–46.
6. Ma Y, Yabluchanskiy A, Hall ME, Lindsey ML. Using plasma matrix metalloproteinase-9 and monocyte chemoattractant protein-1 to predict future cardiovascular events in subjects with carotid atherosclerosis. Atherosclerosis. 2014;232:231–3.

7. Hemingway H, Asselbergs FW, Danesh J, Dobson R, Maniadakis N, Maggioni A, et al. Big data from electronic health records for early and late translational cardiovascular research: Challenges and potential. Eur Heart J. 2018;39:1481–95.
8. Lee GY, Kim JH, Choi KY, Yoon HY, Kim K, Kwon IC, et al. Hyaluronic acid nanoparticles for active targeting atherosclerosis. Biomaterials. 2015;53:341–8.
9. Wu Z, Chen C, Zhang B, Tang L, Shi W, Liao D, et al. EGFP-EGF1-conjugated poly(lactic-co-glycolic acid) nanoparticles, a new diagnostic tool and drug carrier for atherosclerosis. Int J Nanomedicine. 2019;14:2609–18.
10. Bejarano J, Navarro-Marquez M, Morales-Zavala F, Morales JO, Garcia-Carvajal I, Araya-Fuentes E, et al. Nanoparticles for diagnosis and therapy of atherosclerosis and myocardial infarction: Evolution toward prospective theranostic approaches. Theranostics. 2018;8:4710–32.
11. Schiener M, Hossann M, Viola JR, Ortega-Gomez A, Weber C, Lauber K, et al. Nanomedicine-based strategies for treatment of atherosclerosis. Trends Mol Med. 2014;20:271–81.
12. Chan CKW, Zhang L, Cheng CK, Yang H, Huang Y, Tian XY, et al. Recent Advances in Managing Atherosclerosis via Nanomedicine. Small. 2018;14:1–16.
13. Yan F, Sun Y, Mao Y, Wu M, Deng Z, Li S, et al. Ultrasound molecular imaging of atherosclerosis for early diagnosis and therapeutic evaluation through leucocyte-like multiple targeted microbubbles. Theranostics. 2018;8:1879–91.
14. Majmudar MD, Yoo J, Keliher EJ, Truelove JJ, Iwamoto Y, Sena B, et al. Polymeric nanoparticle PET/MR imaging allows macrophage detection in atherosclerotic plaques. Circ Res. 2013;112:755–61.
15. Safavy A, Raisch KP, Mantena S, Sanford LL, Sham SW, Krishna NR, et al. Design and development of water-soluble curcumin conjugates as potential anticancer agents. J Med Chem. 2007;50:6284–8.
16. Sun M, Su X, Ding B, He X, Liu X, Yu A, et al. Advances in nanotechnology-based delivery systems for curcumin. Nanomedicine. 2012;7:1085–100.
17. Maruf A, Wang Y, Yin T, Huang J, Wang N, Durkan C, et al. Atherosclerosis Treatment with Stimuli-Responsive Nanoagents: Recent Advances and Future Perspectives. Adv Healthc Mater. 2019;8:1–28.
18. Cabral H, Miyata K, Osada K, Kataoka K. Block Copolymer Micelles in Nanomedicine Applications. Chem Rev. 2018;118:6844–92.
19. Rösler A, Vandermeulen GWM, Klok HA. Advanced drug delivery devices via self-assembly of amphiphilic block copolymers. Adv Drug Deliv Rev. 2012;64:270–9.
20. Cabral H, Kataoka K. Progress of drug-loaded polymeric micelles into clinical studies. J Control Release. 2014;190:465–76.
21. Hu X, Jing X. Biodegradable amphiphilic polymer-drug conjugate micelles. Expert Opin Drug Deliv. 2009;6:1079–90.

22. Zhu X, Xie H, Liang X, Li X, Duan J, Chen Y, et al. Bilayered Nanoparticles with Sequential Release of VEGF Gene and Paclitaxel for Restenosis Inhibition in Atherosclerosis. ACS Appl Mater Interfaces. 2017;9:27522–32.
23. Zhang K, Tang X, Zhang J, Lu W, Lin X, Zhang Y, et al. PEG-PLGA copolymers: Their structure and structure-influenced drug delivery applications. J Control Release. 2014;183:77–86.
24. Li C, Li W, Liu H, Zhang Y, Chen G, Li Z, et al. An Activatable NIR-II Nanoprobe for In Vivo Early Real-Time Diagnosis of Traumatic Brain Injury. Angew Chemie - Int Ed. 2020;59:247–52.
25. Phinikaridou A, Andia ME, Lacerda S, Lorrio S, Makowski MR, Botnar RM. Molecular MRI of atherosclerosis. Molecules. 2013;18:14042–69.
26. Van Tilborg GAF, Vucic E, Strijkers GJ, Cormode DP, Mani V, Skajaa T, et al. Annexin A5-functionalized bimodal nanoparticles for MRI and fluorescence imaging of atherosclerotic plaques. Bioconjug Chem. 2010;21:1794–803.
27. Cormode DP, Briley-Saebo KC, Mulder WJM, Aguinaldo JGS, Barazza A, Ma Y, et al. An ApoA-I mimetic peptide high-density-lipoprotein-based MRI contrast agent for atherosclerotic plaque composition detection. Small. 2008;4:1437–44.
28. Kheirolomoom A, Kim CW, Seo JW, Kumar S, Son DJ, Gagnon MKJ, et al. Multifunctional Nanoparticles Facilitate Molecular Targeting and miRNA Delivery to Inhibit Atherosclerosis in ApoE-/- Mice. ACS Nano. 2015;9:8885–97.
29. Mlinar LB, Chung EJ, Wonder EA, Tirrell M. Active targeting of early and mid-stage atherosclerotic plaques using self-assembled peptide amphiphile micelles. Biomaterials. 2014;35:8678–86.
30. Bennett MR, Sinha S, Owens GK. Vascular Smooth Muscle Cells in Atherosclerosis. Circ Res. 2016;118:692–702.
31. Wang Y, Zhang K, Qin X, Li T, Qiu J, Yin T, et al. Biomimetic Nanotherapies: Red Blood Cell Based Core–Shell Structured Nanocomplexes for Atherosclerosis Management. Adv Sci. 2019;6.
32. Bruckman MA, Jiang K, Simpson EJ, Randolph LN, Luyt LG, Yu X, et al. Dual-modal magnetic resonance and fluorescence imaging of atherosclerotic plaques in vivo using VCAM-1 targeted tobacco mosaic virus. Nano Lett. 2014;14:1551–8.

Figures

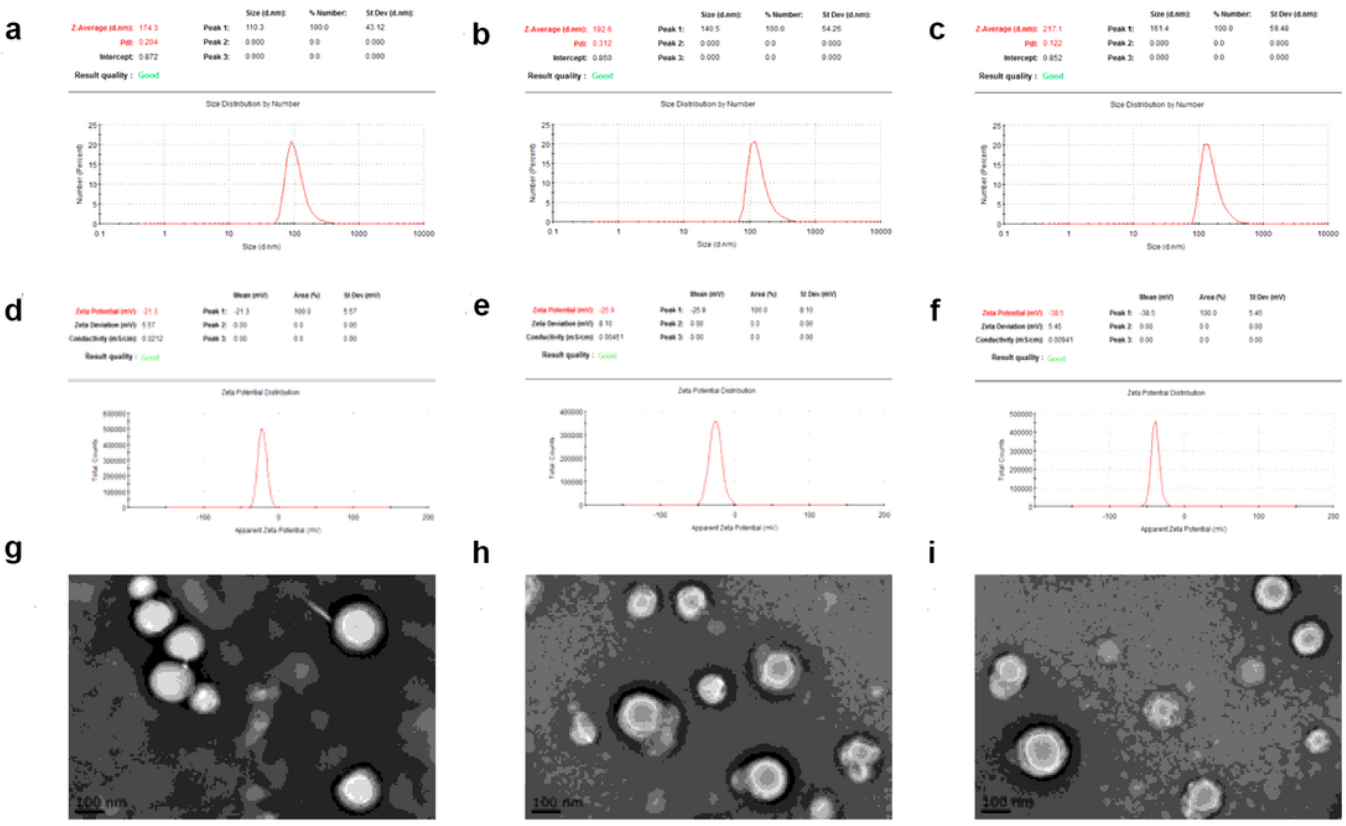

Figure 1

The hydraulic diameter of BPC (a), PCS (b) and PCSV (c) vesicles. Zeta potential of BPC (d), PCS (e) and PCSV (f) vesicles. TEM images of BPC (g), PCS (h) and PCSV (i) vesicles.

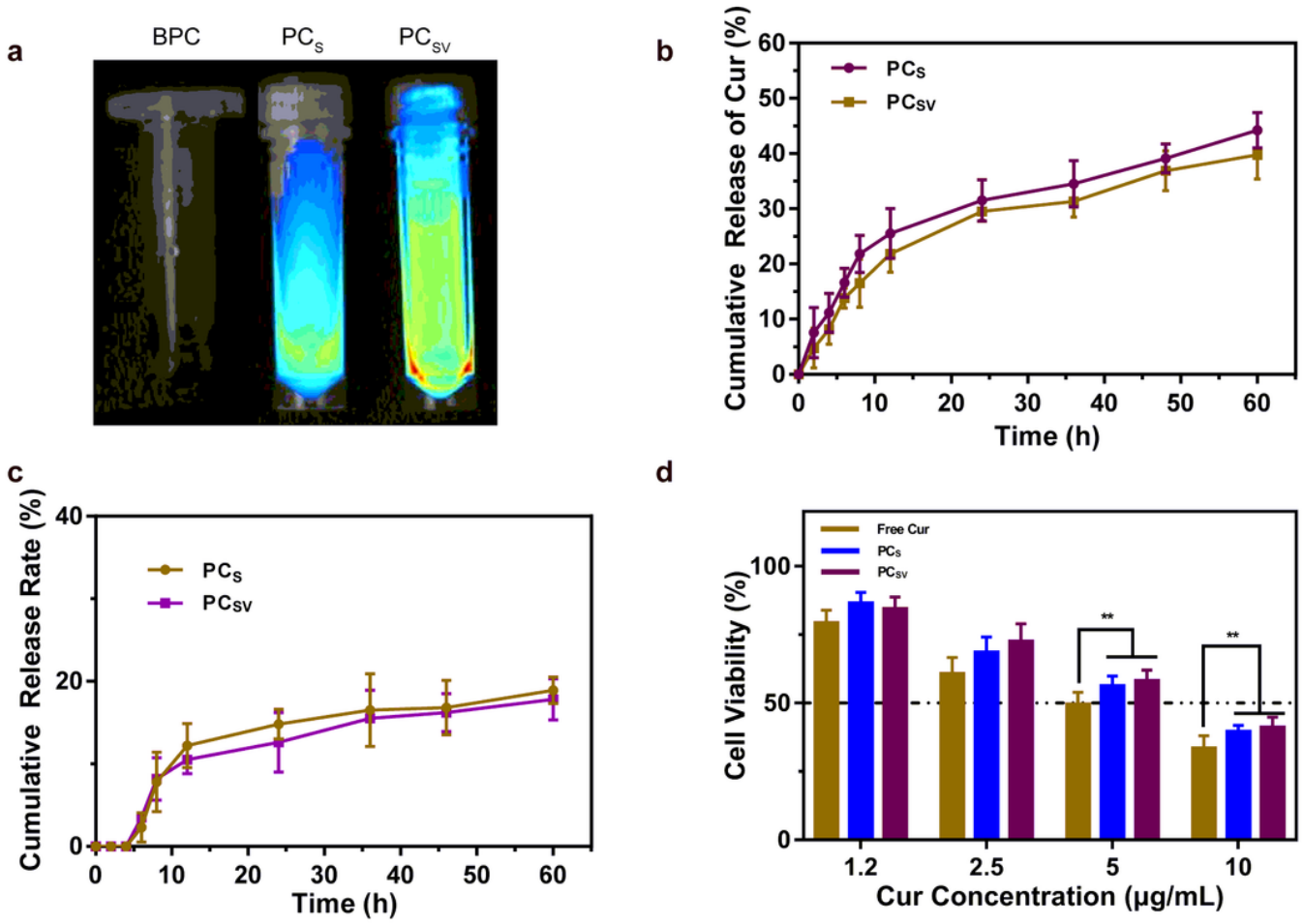

Figure 2

a NIRF imaging of BPC, PCS, and PCSV. b In vitro Cur release profiles of PC and PCV in PBS. c CCR2-siRNA release profiles of PC and PCV in PBS. d Proliferation of RAW264.7 cells after 48 h of incubation with free Cur, PCS and PCSV at different concentration (n = 5).

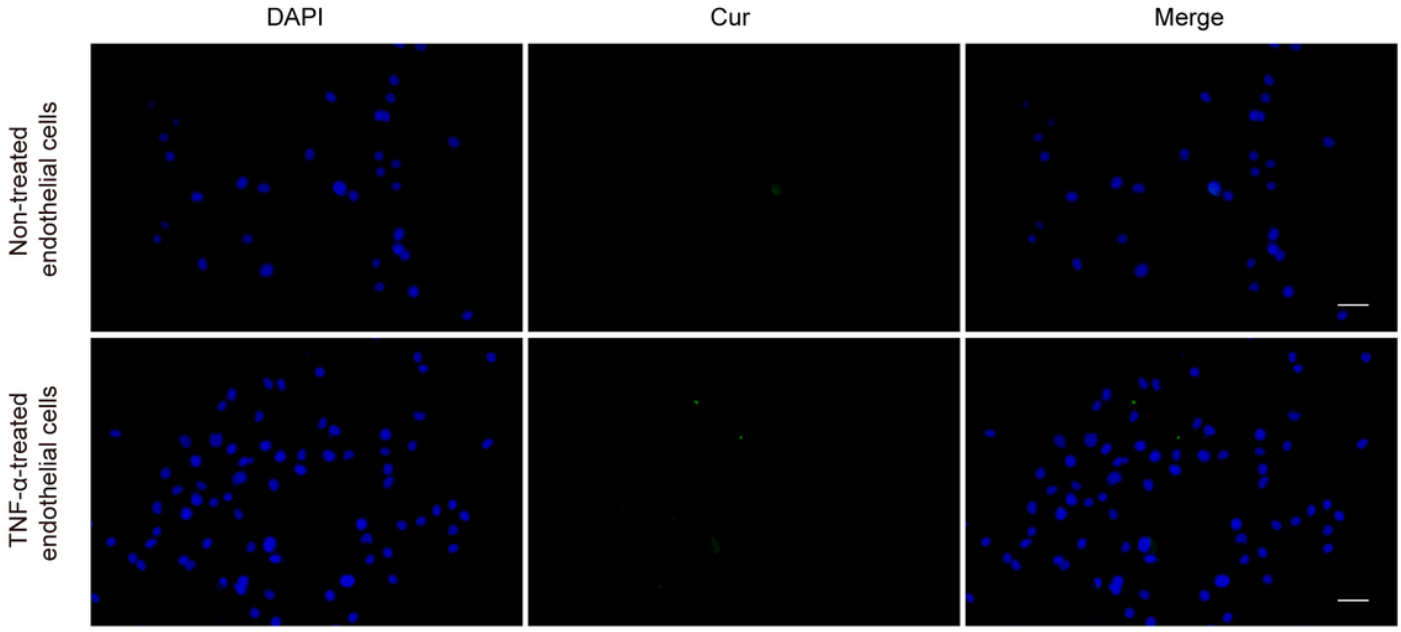

Figure 3

Fluorescence microscopy images of TNF-a-treated endothelial cells and non-treated bEnd.3 cells incubated with PCV (Cur: 2 μg/mL) for 1 h at 37°C. Scale bar=50 μm.

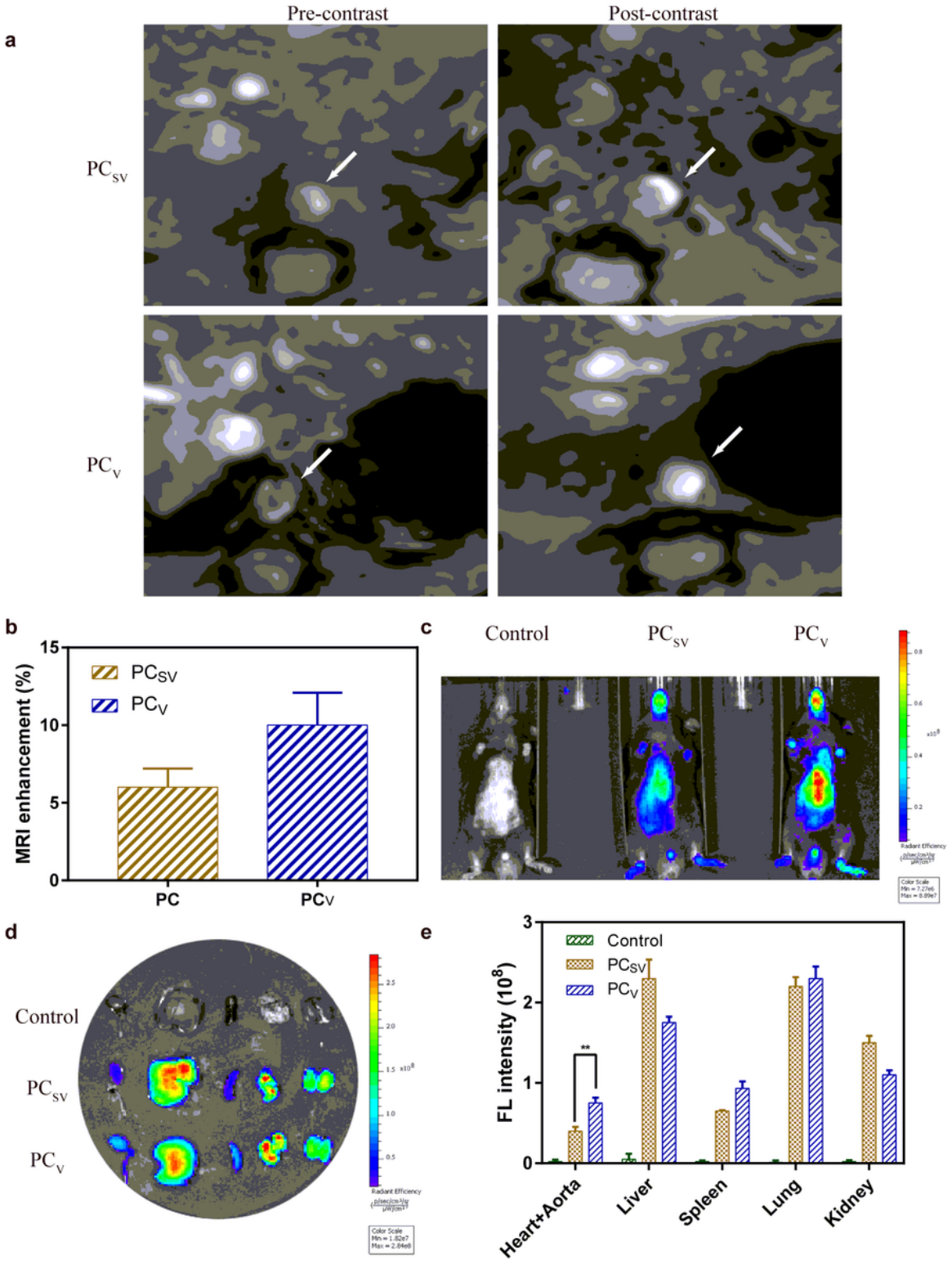

Figure 4

a MRI images of the abdominal aorta, indicated by arrows, of an ApoE-/- mice, before (left) and 24 h post-injection (right) with PCV or PCSV. b Quantitative analysis of MRI signal enhancement in T1-weighted images on day 4 after injection of the contrast agent in ApoE-/- mice. Data represent mean ± SD (n = 4). c In vivo NIRF imaging of ApoE-/-mice intravenously injected with PCV or PCSV after 4 days treatment. d Ex vivo NIRF imaging of the heart and aorta, and other organs collected from the injected ApoE-/- mice after 4 d post-injection. e Quantitative analysis of the heart and aorta, and other organs distribution of NIRF in ApoE-/- mice on day 4 after intravenous injection. Data represent mean ± SD (n = 4).

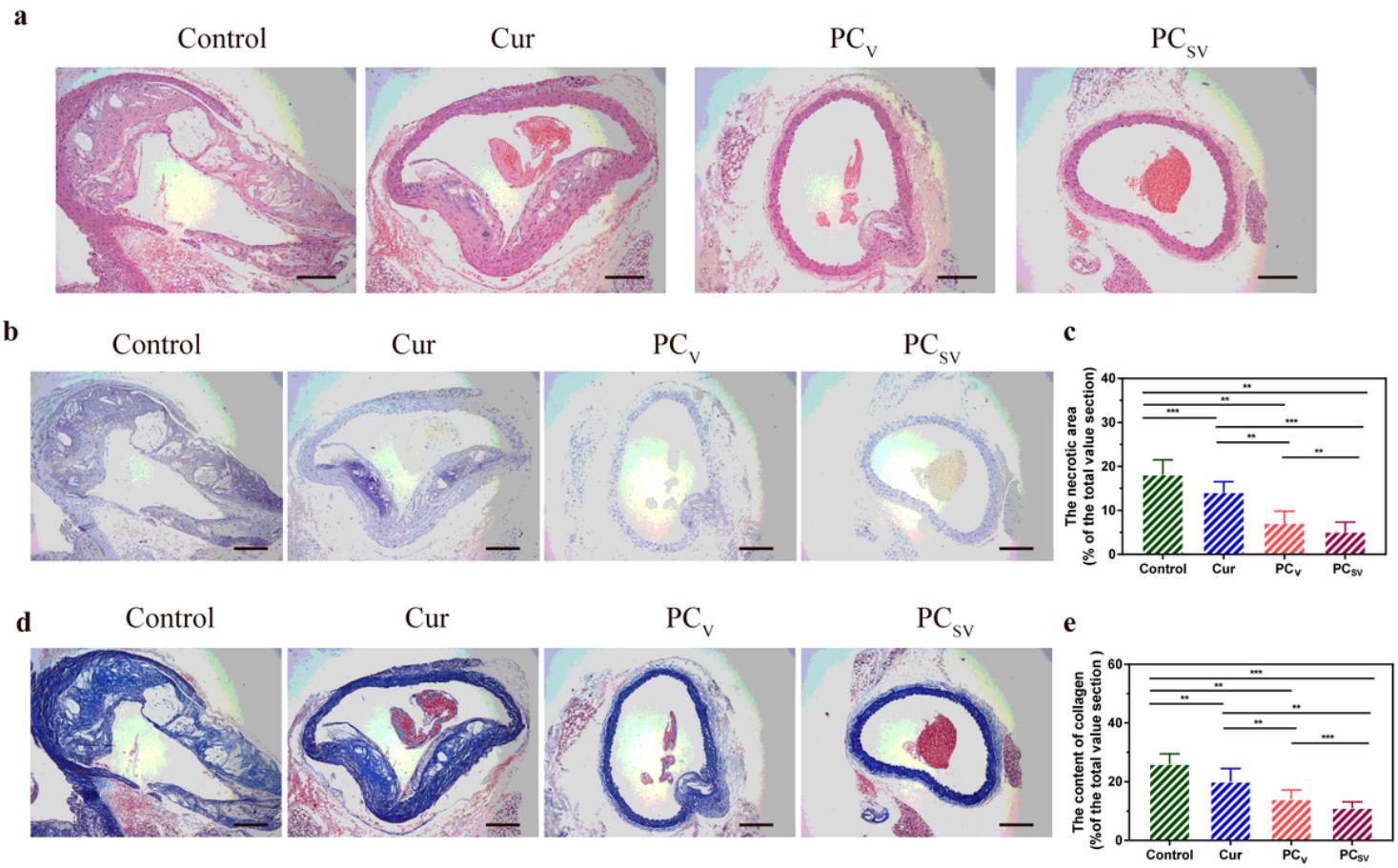

Figure 5

a Representative micrographs of H&E-stained aorta sections from ApoE-/- mice treated with saline, free Cur, PCV, and PCSV for 30 days (scale bar = 500 μm). b The images of the necrotic areas stained by Toluidine blue (scale bar = 500 μm). c Quantitative data of the necrotic areas in the aortic root sections. d The images of collagen in the plaque areas stained by Masson's trichrome (scale bar = 500 μm). e Quantitative data of the content of collagen in aortic root sections. n = 4, mean ± SD, *p < 0.05, **p < 0.01, and ***p < 0.001.

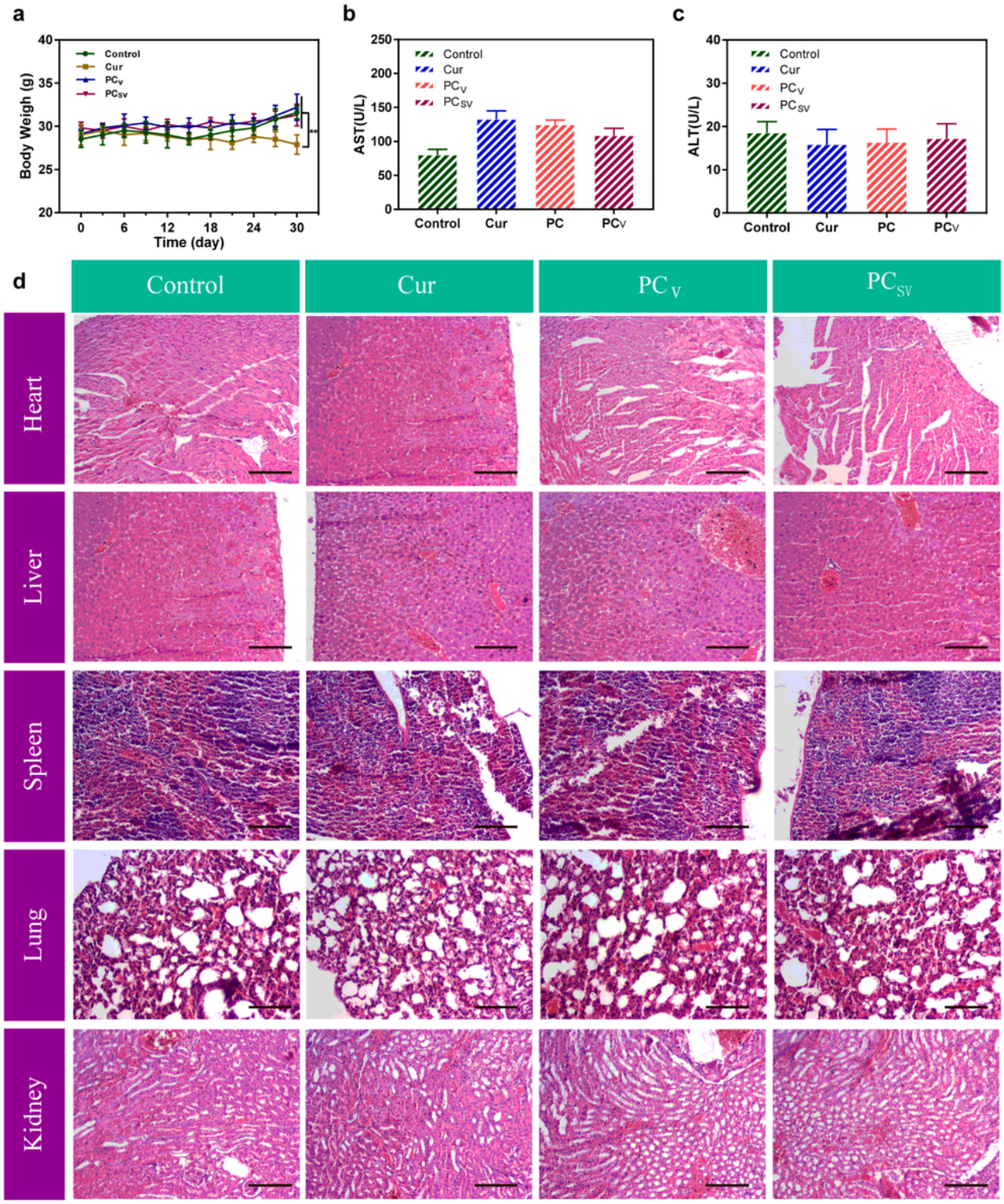

Figure 6

a Effect of different treatments on body weight, Data represents mean ± SD. b The biochemical assays of aspartate aminotransferase (AST). n = 4, mean ± SD. c The biochemical assays of alanine aminotransferase (ALT). n = 4, mean ± SD. d H&E stained images of main organs from mice after various treatments for one month.

Supplementary Files

This is a list of supplementary files associated with this preprint. Click to download.

- Supportinginformation.docx
- Scheme1.png